ORIGINAL PAPER

Computational modeling of muscular thin films for cardiac repair

Markus Böl · Stefanie Reese · Kevin Kit Parker · Ellen Kuhl

Abstract Motivated by recent success in growing biohybrid material from engineered tissues on synthetic polymer films, we derive a computational simulation tool for muscular thin films in cardiac repair. In this model, the polydimethylsiloxane base layer is simulated in terms of microscopically motivated tetrahedral elements. Their behavior is characterized through a volumetric contribution and a chain contribution that explicitly accounts for the polymeric microstructure of networks of long chain molecules. Neonatal rat ventricular cardiomyocytes cultured on these polymeric films are modeled with actively contracting truss elements located on top of the sheet. The force stretch response of these trusses is motivated by the cardiomyocyte force generated during active contraction as suggested by the filament sliding theory. In contrast to existing phenomenological models, all material parameters of this novel model have a clear biophyisical interpretation. The predictive features of the model will be demonstrated through the simulation of muscular thin films. First, the set of parameters will be fitted for one particular experiment documented in the literature. This parameter set is then used to validate the model for various different experiments. Last, we give an outlook of how the proposed simulation tool could be used to virtually predict the response of multi-layered muscular thin films. These three-dimensional constructs show a tremendous regenerative potential in repair of damaged cardiac tissue. The ability to understand, tune and optimize their structural response is thus of great interest in cardiovascular tissue engineering.

Keywords Finite element modeling · Muscle contraction · Micromechanics · Tissue engineering · Cardiovascular tissue repair

M. Böl (✉) · S. Reese
Department of Mechanical Engineering,
Technische Universität Carolo-Wilhelmina,
38106 Braunschweig, Germany
e-mail: m.boel@tu-bs.de

K. K. Parker
Disease Biophysics Group, School of Engineering and Applied
Sciences, Harvard University, Cambridge, MA 02138, USA

E. Kuhl
Departments of Mechanical Engineering and Bioengineering,
Stanford University,
Stanford, CA 94305-4040, USA

1 Motivation

Heart disease is the leading cause of death in industrialized nations. As a result of insufficient blood supply, the functional units of the myocardium, the cardiomyocytes, lose their contractile property and die [21,24]. Unfortunately, in adult tissues such as the heart, the capacity for self regeneration is severely limited: unlike other cell types in the body, cardiomyocytes do not show the potential for self renewal. Recently, stem cell therapy has emerged as a promising methodology for cardiac repair by implanting tissue engineered vascular grafts onto the damaged tissue to restore cardiac function and prevent further onset of deterioration [26,27]. To successfully integrate into the surrounding myocardium, these tissue engineered constructs must possess similar mechanical properties as the implantation site: ideally, they are (i) incompressible, (ii) compliant, (iii) anisotropic, and, most importantly, (iv) contractile.

Due to the tremendous recent developments in stem cell biology it is nowadays possible to differentiate stem cells into cardiomyocytes in vitro, see, e.g., [1]. However, randomly in vitro grown cellular constructs display three essential shortcomings: First, they clearly lack an overall structural organization, i.e., unlike cardiac tissue, they do not possess a

Fig. 1 Laminar myocardium engineered from neonatal ventricular myocytes cultured on a PDMS film with micropatterned fibronectin lines. Phase image of myocytes cultured in 20 mm wide FN lines spaced 20 mm apart (20× magnification)

pronounced direction of fiber orientation. Second, although they might be contractile, their contractility is hardly ever synchronized. Accordingly, they are unable to generate sufficient force during the ejection phase of the cardiac cycle. Third, since cells can only be grown in monolayers in vitro, the shape and form of cardiovascular grafts grown from cells alone is severely limited. These fundamental deficiencies in tissue engineering can be overcome by growing cells on synthetic polymer films. These films allow for mesoscale sculpturing of arbitrary functional forms and give the construct a unique structural integrity. When micropatterned with extracellular matrix proteins, these polymeric base layers can even promote targeted, spatially oriented, two-dimensional myogenesis.

A tremendous break through in cardiovascular tissue engineering was reported just a few months ago when the first prototypes of in vitro grown muscular thin films were presented [13]. Their biohybrid materials consist of a polydimethylsiloxane (PDMS) base layer seeded with synchronously contracting neonatal rat ventricular cardiomyocytes, either spontaneously contractile or externally paced, see Fig. 1. Culturing cardiomyocytes on micropatterned polymeric substrates has tremendous potential in cardiovascular tissue repair since the engineered constructs behave just like the healthy myocardium: they are (i) incompressible, (ii) compliant, (iii) anisotropic, and (iv) contractile. Moreover, all these mechanical properties are fully tunable: incompressibility and compliance are controllable through the properties of the polymeric substrate [12], anisotropy is controllable through micropatterning [13,22] and contractility is controllable through pacing [2].

Rather than varying all the design parameter of cardiovascular tissue grafts in vitro, we propose to develop a finite

element based computational design tool to explore and tune these controllable mechanical parameters in silico. The biohybrid muscular thin films are modeled through a fully hybrid finite element approach. The PDMS substrate is simulated with special three-dimensional finite elements for rubber-like materials that account for both incompressibility and compliance [9]. In these novel elements, the characteristic microstructure of polymers is incorporated through the statistical mechanics of long chain molecules [15,25]. The assembly of the individual chains results in a complex polymeric network that is modeled through the concept of representative volume elements. These elements additionally account for the incompressible behavior of the ground substance on a macroscopic phenomenological level [9].

Anisotropy and active contractility are attributed exclusively to the cardiomyocytes which are located on top of the polymeric base layer. The mechanical properties of cardiac muscle have been well-documented in the literature [5,24]. Their characteristic force stretch response is essentially based on the sliding filament theory [18] which is incorporated constitutively within specifically designed, micromechanically-motivated, non-linear truss elements. Since these elements had originially been developed for skeletal muscle [10,11] they were adapted to simulate cardiac muscle for the present application. The fundamental difference between skeletal and cardiac muscle is that under physiological conditions, skeletal muscle contractile force can be varied by summation of contractions, tetanus and recruitment of additional fibers, whereas cardiac muscle functions as a syncytium such that each cell contracts at every beat [4]. The contractile force in cardiac muscle is thus primarily governed by the current sarcomere length and by the current concentration of intracellular calcium. The binding kinetics of calcium have been studied intensively in the literature, giving rise to excitation-contraction based force contraction models of various complexity [17,23]. However, for the application of in vitro grown muscular thin films addressed within this manuscript, we will assume that the action potential and the calcium concentration are homogeneously distributed within the tissue construct. Accordingly, the contractile force is assumed to depend exclusively on the fiber stretch and on the temporal position within the cardiac cycle. For the resulting one-dimensional cardiac muscle elements, micropatterning-induced anisotropy is then captured inherently through their spatial orientation.

This manuscript is organized as follows. In Sect. 2 we summarize the hybrid computational model for muscular thin films. Section 2.1 and 2.2 describe the finite element model for the polymeric substrate and for the cardiac muscle fibers, respectively. We then illustrate the features of this hybrid model in Sect. 3. Motivated by the recent experimental findings documented in [13], we simulate an unpatterned isotropic circular sheet in Sect. 3.1, three micropatterned

anisotropic rectangular sheets with different fiber orientations in Sect. 3.2, the cylindrial contraction of a coiled strip in Sect. 3.3, and a helical actuator in Sect. 3.4. Section 4 closes with a critical discussion and a final outlook in which we demonstrate that our model is capable to predict the structural response of layered muscular sheets for cardiac repair.
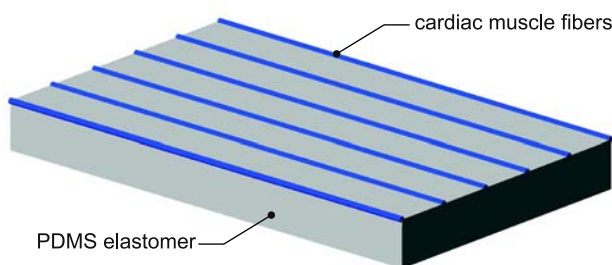
2 Modeling of muscular thin films

For the modeling of muscular thin films, we begin at the microstructural level with a statistical description of single polymer chains. In doing so, we are able to describe polydimethylsiloxane (PDMS) elastomers. In a second step a model is developed to describe the cardiac muscle fibers attached on the surface of the PDMS elastomer films, see Fig. 2.

The elastomer film is represented by means of an assembly of tetrahedral and non-linear truss elements. In each truss element the force stretch behavior of a certain group of polymer chains is implemented. The truss elements are arranged such that each truss is situated on one edge of the finite tetrahedral element to form a tetrahedral unit cell. The tetrahedral element serves to model the incompressible behavior of the elastomer. By using a random assembling procedure we are able to model arbitrary geometries. To account for anisotropy and contractility, bundles of muscle fibers in the form of non-linear truss elements are positioned on top of the PDMS matrix. These trusses contain a mathematical description of the activation at fiber level. By this means we are able to simulate complex muscle structures with arbitrary isotropic or anisotropic fiber distributions.

2.1 The polymeric substrate (PDMS)

The behavior of polydimethylsiloxane elastomers is characterized by large deformations, a non-linear stress-strain relation and incompressibility. To model such a behavior we apply the concept of a tetrahedral unit cell originally developed for rubber-like materials [7–9]. The Helmholtz free energy of one unit cell includes a contribution W^{tet} from the

Fig. 2 Schematic layout of muscular thin films: Cardiac muscle fibers are grown on top of micropatterned elastomer matrix material (PDMS)

tetrahedral element itself, and a contribution W_j^{trs} from the $j = 1, ..., 6$ truss elements situated at the six edges of the tetrahedron.

$$W^{\text{PDMS}}(\mathbf{F}, \lambda_j^{\text{chn}}) = W^{\text{tet}}(\mathbf{F}) + \sum_{j=1}^{6} W_j^{\text{trs}}(\lambda_j^{\text{chn}}). \tag{1}$$

The first term characterizes the volumetric behavior of the unit cell. In detail, W^{tet} reads

$$W^{\text{tet}}(\mathbf{F}) = \frac{K}{4} (J^2 - 1 - 2 \ln J), \tag{2}$$

where $J = \det \mathbf{F}$ denotes the determinant of the macroscopic deformation gradient $\mathbf{F}$ and K is the bulk modulus. Rubber-like materials can be modeled as a three-dimensional network composed of a huge number of macromolecules (also called polymer chains). The micromechanical material behavior of a bundle of polymer chains is characterized by the second term of Eq. (1) and can be specified as

$$W^{\text{trs}}(\lambda^{\text{chn}}) = \frac{\nu^{\text{chn}}}{A_0 L_0} W^{\text{chn}}(\lambda^{\text{chn}}). \tag{3}$$

Herein, A_0 and L_0 are the geometry-dependent cross section and the length of the undeformed truss element, respectively, and ν^{chn} denotes the chain density per truss element, i.e., the ratio $\nu^{\text{chn}} = n^{\text{chn}}/n_{\text{chn}}^{\text{trs}}$ between the number of polymer chains n^{chn} and the number of chain truss elements $n_{\text{chn}}^{\text{trs}}$ in the same reference volume. In the simplest case, one polymer chain can be characterized through n bonds of equal length l. If the directions of the neighboring bonds are completely uncorrelated in the sense that directions for a given bond are of equal probability, this chain type is also called freely jointed chain, see [19,20]. By using the Helmholtz energy function

$$W^{\text{chn}}(\lambda^{\text{chn}}) = k \, n \, \Theta \left[\frac{\lambda^{\text{chn}}}{\sqrt{n}} \beta + \ln \frac{\beta}{\sinh \beta} \right] \tag{4}$$

the behavior of the freely jointed chain is implemented in the proposed model. Herein the Boltzmann's constant $k = 1.3810 \times 10^{-20}$ Nmm/K and the absolute temperature $\Theta = 273$ K are two physically-based parameters. By means of the so-called Langevin function $\mathcal{L}(\beta) = \coth \beta - 1/\beta$, which provides the possibility to derive an expression for the entropy of the single polymer chain, we can express $\beta = \mathcal{L}^{-1}(\lambda^{\text{chn}})$ as the inverse of the Langevin function. Alternatively, β is approximated in the form of a series expansion, for a detailed derivation see [9]. Further, the chain stretch is computed by means of the relation

$$\lambda^{\text{chn}} = \frac{r}{r_0} = \frac{L}{L_0}, \tag{5}$$

whereby r describes the end-to-end distance of the polymer chain in the deformed state and r_0 the same distance in the undeformed case. The fact that the ratios r/r_0 (micro level)

and L/L_0 (macro level) are set equal represents the *micro-to-macro transition* in this modeling concept.

Remark 1 (*Macroscopic parameters A_0 and L_0*) When implemented within a finite element framework, the two parameters A_0 and L_0 of Eq. (3) cancel out of the formulation, see [9]. In so far, it is important to emphasize, that in particular the length L_0 does *not* correlate with the length of the polymer chain bundles. The computational efficiency of the present approach could not compete with classical continuum-based finite element computations if the mesh density would be linked to the geometry of the microstructure.

Remark 2 (*Chain density per truss element ν^{chn}*) It is advantageous to choose the chain density per truss element ν^{chn} as large as possible to minimize the number of elements and consequently maximize the computational efficiency. On the other hand, there is a natural upper limit to the ratio governed by convergence considerations, see [9].

2.2 The cardiac muscle fibers

The unique feature of cardiac muscle in comparison with traditional engineering materials is its ability to contract actively without any mechanical influence from outside. In the present contribution this active contraction is realized through three-dimensional truss elements. The active force in one truss element is assumed to be a function of the fiber stretch $f_\lambda(\lambda^{fib})$ scaled with respect to the temporal position within the cardiac cycle $f_t(t)$.

$$F^{act}(t, \lambda^{fib}) = \nu^{fib} f_t(t) f_\lambda(\lambda^{fib}), \tag{6}$$

Similar to the previous subsection, ν^{fib} denotes the fiber density per truss element, i.e., the ratio $\nu^{fib} = n^{fib}/n_{fib}^{trs}$ between the number of fibers n^{fib} and the number of fiber trusses n_{fib}^{trs} per reference cross section.

The guiding idea of this approach is to model the forces produced by single fibers in dependence on the according frequency. The mechanical response initiated by a motoneuron discharge is a single motor unit twitch, as schematically depicted in Fig. 3. The time-dependent function

$$f_t(t) = P \frac{t}{T} \exp\left(1 - \frac{t}{T}\right) \tag{7}$$

describes the twitch in dependence of the twitch force P and the twitch contraction time T. The force versus stretch relation $f_\lambda(\lambda^{fib})$ is often displayed as a piecewise linear function, see also Fig. 4.

For computational reasons, we suggest the use of a smooth function as suggested in [6]. It is given by the following approximation.
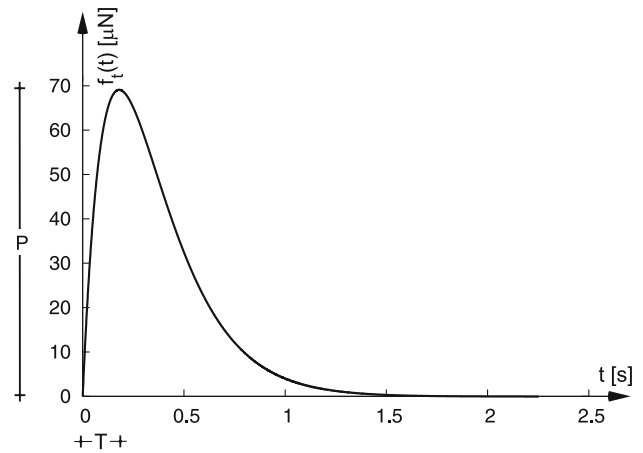
Fig. 3 Isometric single twitch: The force amplitude of the single twitch is controlled by the biophysically-motivated parameters P and T, respectively. Typical values for muscular thin films are $P = 69.1 \, \mu N$ and $T = 180 \, ms$, see [14]
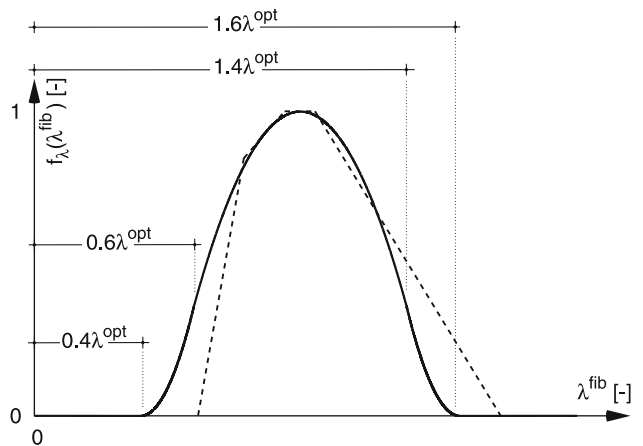

Fig. 4 Stretch function: Piecewise linear function (*dashed curve*) and continuous function

$$f_\lambda(\lambda^{fib}) = \begin{cases} 0, & \lambda^{fib} < 0.4\,\lambda^{opt} \\[2mm] 9\left(\dfrac{\lambda^{fib}}{\lambda^{opt}} - 0.4\right)^2, & 0.6\,\lambda^{opt} > \lambda^{fib} \geq 0.4\,\lambda^{opt} \\[2mm] 1 - 4\left(1 - \dfrac{\lambda^{fib}}{\lambda^{opt}}\right)^2, & 1.4\,\lambda^{opt} > \lambda^{fib} \geq 0.6\,\lambda^{opt} \\[2mm] 9\left(\dfrac{\lambda^{fib}}{\lambda^{opt}} - 1.6\right)^2, & 1.6\,\lambda^{opt} > \lambda^{fib} \geq 1.4\,\lambda^{opt} \\[2mm] 0, & \lambda^{fib} \geq 1.6\,\lambda^{opt} \end{cases} \tag{8}$$

In this formulation, only one dimensionless constant is used, namely λ^{opt}. It defines the optimal fiber stretch at which the sarcomere reaches its optimal length. This is of significant advantage in comparison to the piecewise linear function which requires five material parameters.

Fig. 5 MTF in diastole (**a**) and systole (**b**). The muscle tissue consists of parallel lines of serially aligned neonatal ventricular myocytes cultured on a PDMS film with micropatterned fibronectin lines. Reprinted and modified from [13] with permission
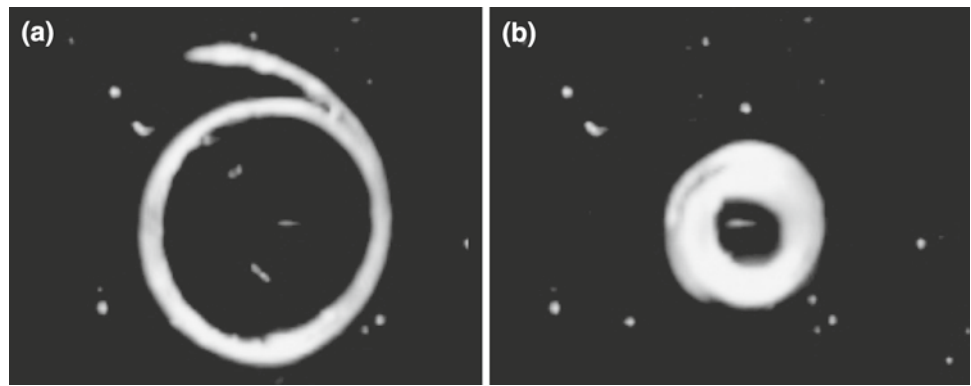
Remark 3 (*Fiber density per truss element ν^{fib}*) It is well-known from experimental observations that the number of cardiac muscle fibers can differ significantly. Therefore it is virtually impossible to discretise *each* muscle fiber only by *one* truss element. In the present approach, each truss element contains n^{fib}/n_{fib}^{trs} truss elements as indicated in Eq. (6).

Remark 4 (*Force vs. time stretch relation*) The active contractile force of both skeletal and cardiac muscles strongly depends on the overlap between actin and myosin filaments, see e.g. [3,16]. However, the stretch-tension relationship for cardiac muscles rises more steeply than for skeletal muscles, cp. [4]. In cardiac muscle, the force stretch relation is often related to the Starling law of the heart.

3 Simulation of muscular thin films

The aim of this section is the study of the deformation behavior of muscular thin films as depicted in Fig. 5. First, we demonstrate an experimental validation of our model for single-layer sheets of muscular thin films. We then provide an outlook showing how the model could be applied to predict the response of multi-layered sheets. In detail the following aspects are analyzed:

- the influence of unpatterned surfaces, i.e. an *isotropic* fiber distribution, on thin film contractility (Sect. 3.1)
- the influence of micropatterned surfaces, i.e. an *anisotropic* fiber distribution, on thin film contractility; parameter identification and model validation (Sect. 3.2)
- possible applications of muscular thin films in the range of actuator modeling with most diverse functionalities (Sect. 3.3 and 3.4)
- the influence of multi-layered muscular sheets on the structural response (Sect. 4)

For all simulations, we use the material parameters as given in [13]. Herein the Young's modulus of Sylgard 184
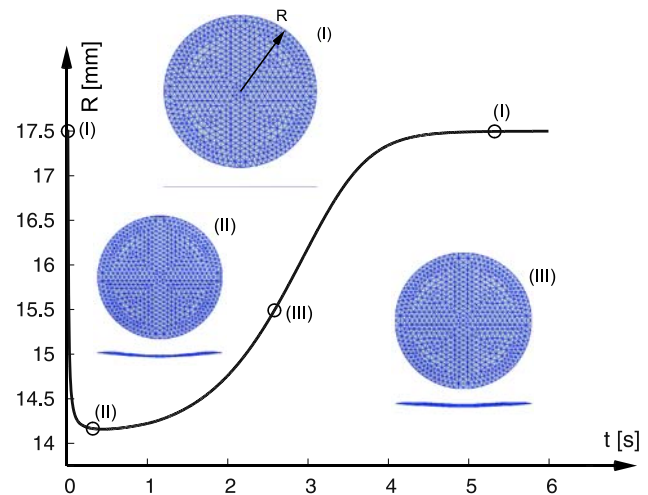
Fig. 6 Circular sheet with isotropic fiber orientation: Three different deformation states depending on the radius R. Shown is the *top view* and the *side view* ($n_{chn}^{trs} = 20, 400 \text{ mm}^{-3}, n_{fib}^{trs} = 120 \text{ mm}^{-2}$)

PDMS is specified by $E = 1.5$ MPa. For our unit cell approach, this stiffness translates to $K = 10^6 \text{ N/mm}^2$, $n = 9$ and $n^{chn} = 7.3 \times 10^6 \text{ mm}^{-3}$. For the characterization of the neonatal rat ventricular cardiomyocytes we identify the twitch force to $P = 69.1 \text{ }\mu\text{N}$, the twitch contraction time to $T = 180$ ms and the number of fibers per unit cross sectio to $n^{fib} = 2.05 \times 10^4 \text{mm}^{-2}$. This basic set of parameters is identical for all simulations. It has been fitted with respect to one single displacement time response of a rectangular sheet to be illustrated in Fig. 7a. The other experiments in Fig. 7b and c were then basically used to validate this data set. The remaining two parameters n_{chn}^{trs} and n_{fib}^{trs} are geometric parameters related to the finite element discretization. For the sake of clarity we neglect the illustration of the truss elements of the polymeric network and restric the illustration to the tetrahedral elements of the polymeric substrate. In addition, we will display the truss elements of the muscular fibers.

Remark 5 (*Boundary conditions and geometry*) One of the most critical issues in biomechanics is the choice of realistic boundary conditions. In the majority of cases, the choice of boundary conditions is a compromise between reality and simulation. Therefore, and for a clearer structure of this manuscript, the choice of the boundary conditions as well as the geometrical dimensions of single structures are given in the appendix, see Sect. 4.

### 3.1 Circular sheet with isotropic fiber orientation

In the first analysis we study the contraction mechanism of a circular muscular sheet. This sheet is assumed to be randomly grown on an unpatterned substrate in a circular petri dish with a diamter of 35mm. Accordingly, the fibers are oriented isotropically on top of the polymeric layer, see Fig. 6.

Due to the isotropic distribution of the cardiac muscle fibers, the sheet contracts isotropically during the activation phase. In-plane isotropy is confirmed through the time sequence (I)–(III) of Fig. 6. In the undeformed state (I) the sheet has its full initial radius of 17.5 mm and shows a non-arched, planar cross-section. In the case of full contraction (III) the radius is reduced to around 14 mm. As expected, during contraction, the sheet experiences out-of-plane deformation towards the contractile cardiomyocyte side. However, the sheet maintains its overall circular shape, what is an indicator for an isometric deformation behavior.

3.2 Rectangular sheets with anistropic fiber orientation

For the validation of our model, three rectangular muscular thin films with different anisotropic fiber orientation were generated. The displacement time curve of the first sheet in Fig. 7a was used to fit the microscopic material parameter set. The curves of the two other sheets Fig. 7b and c can be understood as model validation. Remarkably, the parameters fitted for the first sheet generate simulation results that are almost identical to the experimental findings. Recall that the different parameters $n_{\text{chn}}^{\text{trs}}$ and $n_{\text{fib}}^{\text{trs}}$ used for the three sheets are no arbitrary fitting parameters. Rather, they have a clear geometric interpretation related to the microstructural geometry.

In the first example the cardiomyocytes are aligned in *x*-direction, transversely to the center-line, cp. Fig. 7a. As expected, the sheet bends about the *y*-axis perpendicular to the direction of the cardiac fibers. Due to the short fiber length, the bending is not as pronounced as in the second example, see (b). At time (II) of Fig. 7b the sheet achieves its maximum bending, which leads to an out-of-plane displacement of approximately 1.1 mm. In the third example the fibers are arranged diagonally on the polymer substrate, see Fig. 7c.
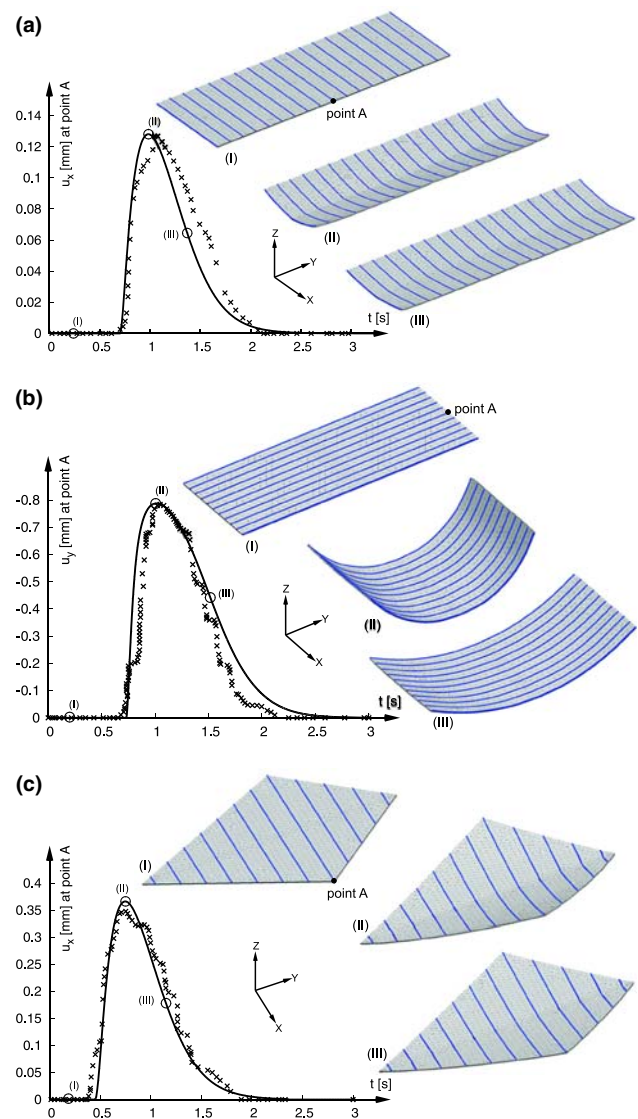
Fig. 7 Muscular thin film (*crosses* experiment, *line* simulation): **a** Cardiomyocytes oriented along the *x*-axis ($n_{\text{chn}}^{\text{trs}} = 150,707 \text{ mm}^{-3}$, $n_{\text{fib}}^{\text{trs}} = 122 \text{ mm}^{-2}$), **b** cardiomyocytes oriented along the *y*-axis ($n_{\text{chn}}^{\text{trs}} = 150,032 \text{ mm}^{-3}$, $n_{\text{fib}}^{\text{trs}} = 71 \text{ mm}^{-2}$) and **c** cardiomyocytes oriented diagonally ($n_{\text{chn}}^{\text{trs}} = 262,240 \text{ mm}^{-3}$, $n_{\text{fib}}^{\text{trs}} = 103 \text{ mm}^{-2}$)

When comparing the deformed shapes of all three sheets it is obvious that the maximum structural deformation is generated for example (b). Sheet deformations reflect the influence of the microstructural arrangement on the overall structural response; different cardiomyocyte orientations result in completely different macroscopic deformation patterns.

In summary it can be seen, that the presented model displays the experimental finding in a excellent manner. Especially the fact, that all three examples are calculated by only *one* parameter set, emphasizes the performance of the our modeling concept. In addition, the model is able to describe
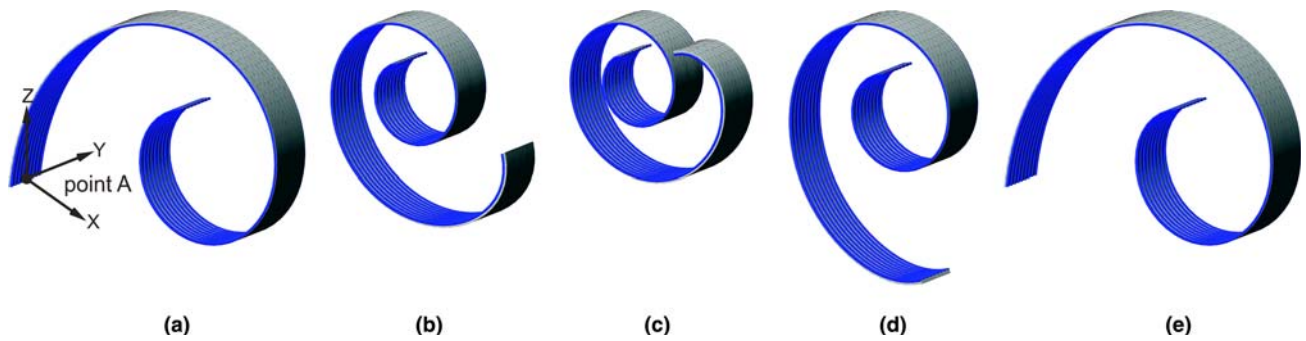
Fig. 8 Five screen shots of coiled strip: **a** Undeformed coil, **b** configuration of the coil between the undeformed (**a**) and the maximum deformed state (**c**), (**d**) shape of coil during relaxation and (**e**) coil shape after contraction process ($n_{chn}^{trs} = 17,775$ mm^{-3}, $n_{fib}^{trs} = 227$ mm^{-2})

a fast contraction followed by a slow relaxation. This temporal asymmetry was also observed in the experiments.

3.3 Cylindrical contraction of coiled strip

Cultured muscular thin films are attractive materials to building actuators and powering devices. Thus, in this section we study the deformation behavior of a coiled strip.

We focus on the large movement of the strip with relation to its function and adaptability as motile soft device. The cardiomyocytes are longitudinally aligned at the inner surface of the rectangular substrate, see Fig. 8. The given time sequence illustrates an (a) initial loosely rolled state, (c) a more tightly rolled shape, (e) the return to the undeformed configuration, and intermediate states (b) and (d). This simulation is conducted during spontaneous contraction for one single twitch.

For all three space direction, the position of point A, cp. Fig. 8a was measured during the simulation. Its temporal evolution is depicted in Fig. 9. Moreover, the five specific positions of point A at times (a)–(e) are indicated. This example demonstrates the incredibly large motion of the coil that is generated by a maximum myocyte contraction of only 15%. The largest deformations in x- and z-direction are approximately 10 mm and 4 mm, respectively. Note that point A does not deform in y-direction due to the choice of boundary conditions, see Sect. 4. This example illustrates that a significant rotation can be generated by this specific arrangement of cardiomyocytes. It is thus straightforward to tune the thin film by orienting the cardiomyocytes in a different direction to generate different structural deformation patterns.

3.4 Helical actuator

Last, we will simulate a helical actuator capable of axial contraction in combination with a rotational movement. The fibers are aligned between 0° and 10° off-line to the length of the PDMS substrate (see inset of Fig. 11).
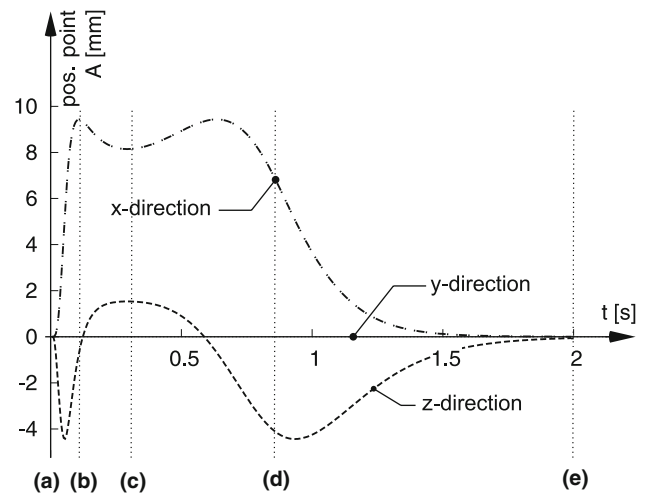

Fig. 9 Position measurement of point A (cp. Fig. 8). **a**–**e** indicate the different shapes of the coiled sheet, cp. Fig. 8
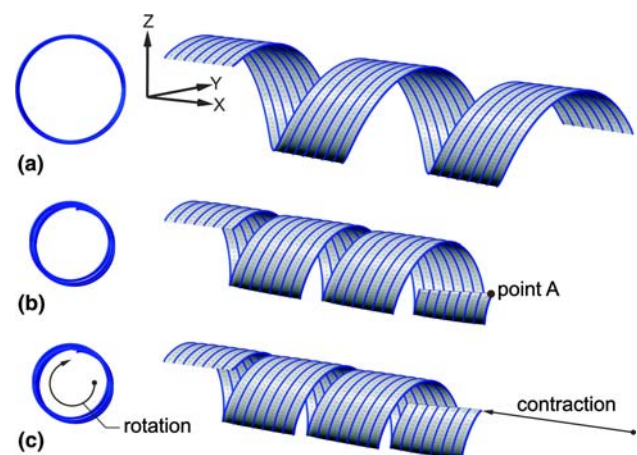
Fig. 10 Helical actuator *left* cross section, *right* side view) fixed on the left end: **a** Undeformed shape, **b** deformed structure during contraction process and **c** maximum deformation ($n_{chn}^{trs} = 205,834$ mm^{-3}, $n_{fib}^{trs} = 227$ mm^{-2})

In Fig. 10 the result of the finite element simulation is illustrated, where an off-line angle of 0° was chosen. In (a) the undeformed structure is shown and (c) characterizes the
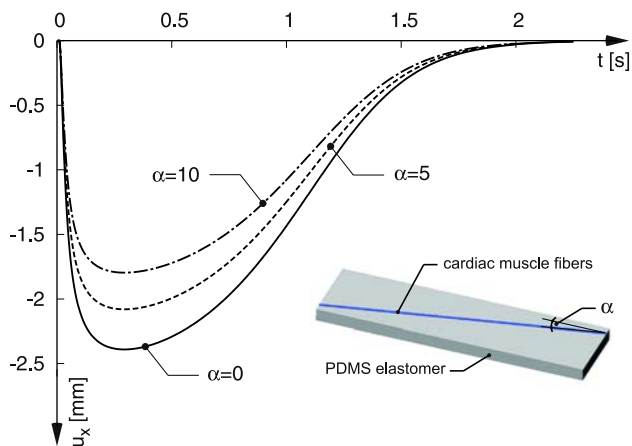
Fig. 11 Influence of different muscle fiber angles α on the maximum longitudinal displacement of the helical actuator as sketched in Fig. 10

maximum deformed configuration. Frame (b) displays an intermediate state between (a) and (c). When tracking point A it is obvious that the actuator movement is governed by a decrease in length and a superposed rotation, see arrows in Fig. 10c. Intuitively, this overall deformation pattern based on a structural contraction during systole and an elongation during diastole seems correct. The in vitro studies, however, report elongation during systole and contraction during diastole. We postulate that this mismatch is caused by the lack for pre-stress in the computational simulation tool in silico whereas significant pre-stress is generated during the fabrication process of the muscular thin films in vitro.

Finally, we investigate the influence of the off-line angle. The inset of Fig. 11 schematically illustrates the definition of the angle α. Simulations with three different angles ($\alpha = 0°/5°/10°$) were conducted. Figure 11 shows the maximum decrease in length (*x*-direction). The maximum displacement is reached for an off-line angle of $\alpha = 0°$, i.e., with all fibers aligned with the sheet axis. Increasing the off-line angles obviously reduces the overall contraction length. The results of a systematic variation of fiber orientation can be used as a numerical tool to control and tune the deformation behavior of an actuator. The proposed modeling approach enables the prediction of the structural response as a function of cardiomyocyte orientation with respect to the PDMS substrate.

4 Discussion and outlook

Motivated by the recent success in growing actively contracting cardiomyocytes on micropatterned polymeric substrates, we developed a computational simulation tool that allows the systematic prediction of tissue engineered biohybrid materials for cardiac repair. The incompressible, compliant polydimethylsiloxane base layer has been simulated with representative tetrahedral unit cell elements. Neonatal rat

ventricular cardiomyocytes grown on top of this layer have been simulated with actively contracting truss elements. Random orientations of these truss elements have been used to generate unpatterend isotropic structures, whereas aligned truss elements have been applied to simulate micropatterned anisotropic structures. Starling's law of the heart has been applied to motivate the force stretch relationship for cardiomyocytes on the microscopic level. To account for the temporal position within the cardiac cycle, the force stretch relationship has been weighted by the temporal evolution of force during an isometric single twitch. Micro-to-macro transition is performed via homogenization schemes introducing geometric scaling parameters that represent the number of polymer chains and fibers per truss finite element. A unique advantage of the proposed microscopically-motivated model in comparison to macroscopic-phenomenologic models is that its material parameters have a clear biophysical interpretation.

A series of examples was presented to illustrate the features of the suggested approach. The proposed model has been shown capable of reproducing the experimental results of in vitro grown muscular thin films. Qualitative and quantitative validations have demonstrated the potential of the proposed approach in modeling actively contracting cardiovascular tissue. An open question to be addressed in the futures is the incorporation of pre-stress. We anticipate that the incorporation of pre-stress induced during the tissue engineering process is essential to characterize complex structural geometries like the helix which expands during systole and contracts during diastole in vitro whereas it displays the opposite behavior in silico. We are currently working on enhancing our theory to explore the influence of pre-stress.

An immediate goal of this research project it to provide guidelines to optimize tissue engineered patches in cardiac repair. The muscular thin films grown by the Harvard group provide a first step in this direction. However, from a practical point of view, their muscular films might be too thin to be implantable onto the damaged myocardium. In an attempt to mimic the true cardiac microstructure, cardiovascular tissue engineers seek to produce stacks of multiple muscular thin films. The unique advantage of a computational simulation tool is that the fiber orientation in each layer can be optimized in silico and tuned with respect to the fiber orientation close to the potential implantation site. To demonstrate the computationally guided design of multi-layered patches for cardiac repair, we virtually staple three representative sheets with different fiber orientations and explore the overall structural response of the tissue patch. Figure 12 displays four different time sequences within a cardiac cycle for a representative three-layer sheet with line-off angles of 60°, 0° and −60°. The structural response clearly reflects a superposition of tension and torsion characteristic for the contracting heart.
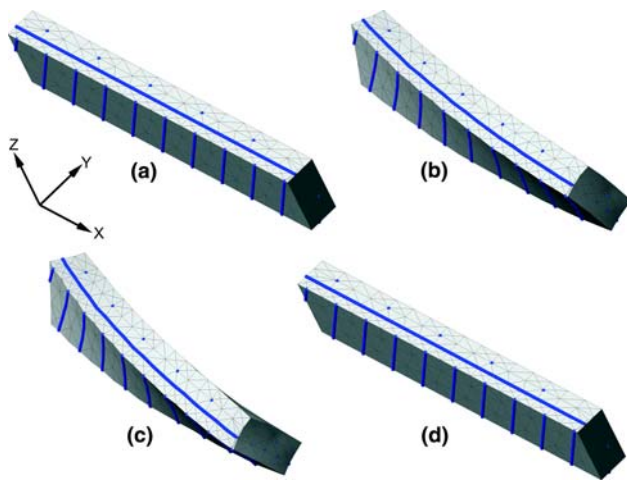
Fig. 12 Multi-layer sheet with three single sheets of fiber alignment $(60°/0°/-60°)$: Four screen shots for one contraction circle. **a** Undeformed structure before contraction, **b** deformed shape between state **a** and **c**, **c** maximum contracted sheets and **d** multi-layer sheets after contraction process ($n_{\text{chn}}^{\text{trs}} = 97,070 \text{ mm}^{-3}$, $n_{\text{fib}}^{\text{trs}} = 56 \text{ mm}^{-2}$)

This example clearly illustrates the potential of the proposed algorithm to improve the design of tissue engineered patches for cardiac repair. Our collaborators in are currently aiming to build these multi-layered patches in vitro. The ultimate goal of this project, however, is to predict the structural integration of these patches when implanted on a real heart with a complex microstructure of clearly defined fiber sheet orientations and compare the results to real in vivo experiments.
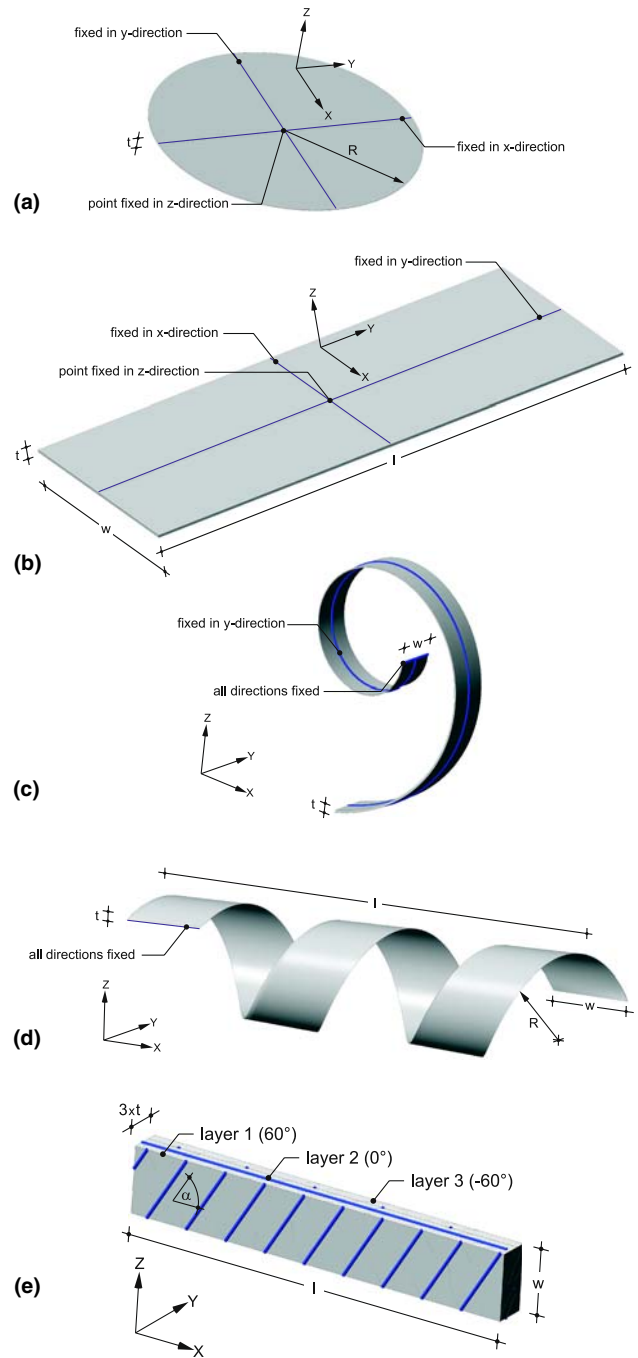
Appendix: Geometry and boundary conditions

This appendix includes the geometry measurements adopted from [13] as well as the boundary conditions of the numerical examples presented in Sect. 3. For all examples we use a thickness of $t = 0.03$ mm. Further in all analyses, with the exception of the multi-layered sheet, we used four finite elements across the sheet thickness.

Sect. 3.1: Circular sheet The circular sheet with isometric fiber distribution, cp. Fig. 13a, has a radius of $R = 17.5$ mm. The sheet is fixed in x-direction at the line aligned with the y-axis and fixed in y-direction aligned with the x-axis. Additional, one point in the center of the sheet is hold in z-direction.

Sect. 3.2: Rectangular sheets The rectangular sheets with anisotropic fiber distributions, cp. Fig. 13b, have the dimensions of $l/w = 5.2/2.5$ mm for the examples of Fig. 7a, b and $l/w = 3.0/2.5$ mm for the sheet of Fig. 7c. The sheets are fixed in x-direction at the line aligned with the y-axis and fixed in y-direction aligned with the x-axis. Additional, one point in the center of the sheet is hold in z-direction.

Sect. 3.3: Coiled strip By the coiled strip, cp. Fig. 13c, the fibers are attached to the inner side of structure. The coil is

Fig. 13 Geometry and boundary conditions of the analyzed structures: Sect. 3.1: Circular sheet with isotropic fiber orientation, Sect. 3.2: Rectangular sheet with anisotropic fiber orientation, Sect. 3.3: Cylindrical contraction of coiled strip, Sect. 3.4: Helical actuator, and Sect. 4: Multilayer sheet

fixed at the inner end in all space directions. To account for symmetric boundary conditions the middle plane is fixed in y-direction. The strip's width measures $w = 1.32$ mm.

Sect. 3.4: Helical actuator In this example, cp. Fig. 13d, the fibers are arranged to the inner side of the helix. The

structure is fixed at the left end in all space directions. The measurements are $R/l/w = 1.0/7.7/1.32$ mm.

Sect. 4: Multi-layer sheet Three sheets are use to build up the multi-layer sheet, cp. Fig. 13e. The three single sheets have different line-off angles (layer1/2/3=$60°/0°/-60°$). The fibers are attached on one side of each layer only. The multi-layer sheet is fixed in the center of the second layer at four points in all space directions. The measurements are $l/w = 1.1/0.18$ mm.

References

1. Abilez O, Benharash P, Mehrotra M, Miyamoto E, Gale A, Picquet J, Xu C, Zarins C (2006) A novel culture system shows that stem cells can be grown in 3D and under physiologic pulsatile conditions for tissue engineering of vascular grafts. J Surg Res 132:170–178

2. Abilez O, Benharash P, Miyamoto E, Gale A, Xu C, Zarins CK (2006) P19 progenitor cells progress to organized contracting myocytes after chemical and electrical stimulation: Implications for vascular tissue engineering. J Endovasc Ther 13:377–388

3. Allen DG, Jewell BR, Murray JW (1974) The contribution of activation processes to the length-tension relation of cardiac muscle. Nature 248:606–607

4. Bers DM (2001) Excitation-contraction coupling and cardiac contractile force. Springer, Berlin

5. Bers DM (2002) Cardiac excitation contraction coupling. Nature 415:198–205

6. Blemker SS, Delp SL (2005) Three-Dimensional Representation of Complex Muscle Architectures and Geometries. Ann Biomed Eng 33:661–673

7. Böl M, Reese S (2005) New method for simulation of Mullins effect using finite element method. Plast Rub Comp 34:343–348

8. Böl M, Reese S (2005) Finite element modelling of rubber-like materials—a comparison between simulation and experiment. J Mat Sci 40:5933–5939

9. Böl M, Reese S (2006) Finite element modelling of rubber-like polymers based on chain statistics. Int J Sol Struc 43:2–26

10. Böl M, Reese S (2007) A new approach for the simulation of skeletal muscles using the tool of statistical mechanics. Mat Sci Eng Tech 38:955–964

11. Böl M, Reese S (2008) Micromechanical modelling of skeletal muscles based on the finite element method. Comp Meth Biomech Biomed Eng (in press)

12. Cao F, Sadrzadeh A, Abilez O, Wang H, Pruitt B, Zarins C, Wu J (2007) In vivo imaging and evaluation of different biomatrices for improvement of stem cell survival. J Tissue Eng Regen Med 1:465–468

13. Feinberg AW, Feigel A, Shevkoplyas SS, Sheehy S, Whitesides GM, Parker KK (2007) Muscular thin films for building actuators and powering devices. Science 317:1366–1370

14. Feinberg AW, Feigel A, Shevkoplyas SS, Sheehy S, Whitesides GM, Parker KK (2007) Supporting Online Material for: Muscular thin films for building actuators and powering devices. Science 317:1–17

15. Flory PJ (1969) Statistical Mechanics of Chain Molecules. Wiley, Chichester

16. Gordon AM, Huxley AF, Julian FJ (1966) The variation in isometric tension with sarcomere length in vertebrate muscle fibres. J Phys 184:170–192

17. Hunter PJ, McCulloch AD, ter Keurs JEDJ (1998) Modelling the mechanical properties of cardiac muscle. Prog Biophys Mol Biol 69:289–331

18. Huxley H, Hanson J (1954) Changes in the cross-striations of muscle during contraction and stretch and their structural interpretation. Nature 173:973–976

19. Kuhn W (1934) Über die Gestalt fadenförmiger Moleküle in Lösungen. Kolloid Z 68:2–15

20. Kuhn W (1936) Beziehungen zwischen Molekühlgrösse, statistischer Molekülgestalt und elastischen Eigenschaften hochpolymerer Stoffe. Kolloid Z 76:258–271

21. Kumar V, Abbas AK, Fausto N (2005) Robbins and Cotran pathologic basis of disease. Elsevier, Saunders, Amsterdam, Philadelphia

22. Kurpinkski K, Chu J, Hashi C, Li S (2007) Anisotropic mechanosensing by mesenchymal stem cells. PNAS 103:16095–16100

23. Luo CH, Rudy Y (1991) A dynamic model of the cardiac ventricular action potential: I. Simulations of ionic currents and concentration changes. Circ Res 74:1071–1096

24. Opie LH (2003) Heart Physiology: From Cell to Circulation. Lippincott Williams & Wilkins, Philadelphia

25. Treloar LRG (1975) The Physics of Rubber Elasticity. Clarendon Press, Oxford

26. Wollert KC, Meyer GP, Lotz J, Ringes-Lichtenberg S, Lippolt P, Breidenbach C, Fichtner S, Korte T, Hornig B, Messinger D, Arseniev L, Hertenstein B, Ganser A, DrexlerH Wollert KC, Meyer GP, Lotz J (2004) Intracoronary autologous bone-marrow cell transfer after myocardial infarction: the BOOST randomised controlled clinical trial. Lancet 364:141–148

27. Zimmermann WH, Melnychenko I, Wasmeier G, Didié M, Naito J, Nixdorff U, Hess A, Budinsky L, Brune K, Michaelis B, Dhein S, Schwoerer A, Ehmke H, Eschenhagen T (2006) Engineered heart tissue grafts improve systolic and diastolic function in infarcted rat hearts. Nat Med 124:452–458